

## RESEARCH ARTICLE

10.1029/2017JA025174

## Special Section:

Dayside Magnetosphere Interaction

## Magnetosheath Propagation Time of Solar Wind Directional Discontinuities

A. A. Samsonov<sup>1,2</sup> , D. G. Sibeck<sup>3</sup> , N. P. Dmitrieva<sup>1</sup>, V. S. Semenov<sup>1</sup>, K. Yu. Slivka<sup>1</sup> , J. Šafránková<sup>4</sup> , and Z. Němeček<sup>4</sup> <sup>1</sup>St. Petersburg State University, St. Petersburg, Russia, <sup>2</sup>Mullard Space Science Laboratory, University College London, Holmbury St Mary, UK, <sup>3</sup>NASA Goddard Space Flight Center, Greenbelt, MD, USA, <sup>4</sup>Faculty of Mathematics and Physics, Charles University, Prague, Czech Republic

## Key Points:

- Magnetosheath propagation times decrease with solar wind speed increase
- Magnetosheath propagation times increase with IMF magnitude increase
- Magnetosheath propagation times are slightly smaller for southward IMF

## Correspondence to:

A. A. Samsonov,  
a.samsonov@spbu.ru

## Citation:

Samsonov, A. A., Sibeck, D. G., Dmitrieva, N. P., Semenov, V. S., Slivka, K. Y., Šafránková, J., & Němeček, Z. (2018). Magnetosheath propagation time of solar wind directional discontinuities. *Journal of Geophysical Research: Space Physics*, 123, 3727–3741. <https://doi.org/10.1029/2017JA025174>

Received 31 DEC 2017

Accepted 10 APR 2018

Accepted article online 23 APR 2018

Published online 18 MAY 2018

**Abstract** Observed delays in the ground response to solar wind directional discontinuities have been explained as the result of larger than expected magnetosheath propagation times. Recently, Samsonov et al. (2017, <https://doi.org/10.1002/2017GL075020>) showed that the typical time for a southward interplanetary magnetic field (IMF) turning to propagate across the magnetosheath is 14 min. Here by using a combination of magnetohydrodynamic simulations, spacecraft observations, and analytic calculations, we study the dependence of the propagation time on solar wind parameters and near-magnetopause cutoff speed. Increases in the solar wind speed result in greater magnetosheath plasma flow velocities, decreases in the magnetosheath thickness and, as a result, decreases in the propagation time. Increases in the IMF strength result in increases in the magnetosheath thickness and increases in the propagation time. Both magnetohydrodynamic simulations and observations suggest that propagation times are slightly smaller for northward IMF turnings. Magnetosheath flow deceleration must be taken into account when predicting the arrival times of solar wind structures at the dayside magnetopause.

## 1. Introduction

Solar wind parameters often change in a discontinuous manner, on time scales ranging from several seconds to several minutes. Two large groups of solar wind discontinuities are interplanetary shocks and solar wind directional discontinuities (DDs). Interplanetary shocks usually bring increases in the solar wind dynamic pressure, but also change the interplanetary magnetic field (IMF) magnitude and orientation. Interacting with the magnetosphere, interplanetary shocks significantly disturb the magnetospheric magnetic field, resulting in sudden impulses in ground observations and sometimes initiating geomagnetic storms (see, e.g., Araki, 1994; Kokubun et al., 1977; Nishida, 1992; Samsonov et al., 2015; Tsurutani et al., 2011, and a recent review of Oliveira & Samsonov, 2017).

Within the framework of magnetohydrodynamics (MHD), solar wind DDs can be either tangential or rotational. Since it is often difficult to classify an observed solar wind discontinuity exactly as a tangential or rotational one, we use the generalized term DD throughout this paper (e.g., Smith, 1973). DDs only occasionally change the solar wind dynamic pressure, but they always change the IMF orientation. They may be more geoeffective, if they change the sign of the IMF  $B_z$ . Southward IMF turnings cause the sign of  $B_z$  to change from positive to negative, while northward IMF turnings have the opposite effect. Southward IMF turnings provide optimal conditions for reconnection on the dayside magnetopause and magnetic flux transfer to the magnetotail (Dungey, 1961). Northward IMF turnings may trigger magnetospheric substorms (Hsu & McPherron, 2003, and references therein).

The motion of interplanetary shocks through the magnetosheath and outer magnetosphere has been reasonably well reproduced by MHD simulations (Andréová, 2009; Goncharov et al., 2015; Koval et al., 2005; Koval, Šafránková, Němeček, Samsonov, et al., 2006; Samsonov et al., 2006, 2007). Fast forward shocks require only 1–2 min to cross the magnetosheath along the Sun–Earth line. Shock speeds in the magnetosheath are slightly lower than those in the solar wind (Koval et al., 2005; Koval, Šafránková, Němeček, & Přech, 2006).

The interaction of a solar wind tangential discontinuity with the bow shock can transmit a fast forward shock (fast rarefaction wave) into the magnetosheath, if the solar wind density increases (decreases) through

the tangential discontinuity (Maynard et al., 2007; Völk & Auer, 1974; Wu et al., 1993). However, this shock (rarefaction wave) is weak for small or moderate density changes and completely disappears for solar wind discontinuities with constant density (Wu et al., 1993).

Previous studies (e.g., Bhaskar & Vichare, 2013; Ridley et al., 1998; Ruohoniemi & Greenwald, 1998; Saunders et al., 1992; Taylor et al., 1998; see more references in Samsonov et al., 2017) determined that the delay from a solar wind DD reaching the subsolar bow shock to the first response in ground magnetometers or radars is on the order of 10–16 min. Samsonov et al. (2017) recently used an MHD simulation to study a DD accompanied by a southward turning and showed that the DD propagation time through the magnetosheath was 14 min in good agreement with the ground response seen in changes of the Polar Cap North (PCN) index (Troshichev et al., 2006). Samsonov et al. (2017) noted a significant deceleration of the DD as it approached the magnetopause. The IMF was northward before the DD, and a magnetic barrier (Pudovkin, 1987) formed near the magnetopause. When the discontinuity with a southward IMF turning moved earthward through the magnetosheath, the magnetic barrier was disrupted via magnetic reconnection. The southward turning reached the magnetopause only after a complete dissipation of the magnetic barrier. Finally, it takes only about 1 min from the contact of the DD with the subsolar magnetopause to the first ground (ionospheric) response. During the same event, Samsonov et al. (2017) noted a sunward motion of the subsolar magnetopause for  $\sim 10$  min before the DD had reached the magnetopause. Their MHD simulation showed that the dissipation of the magnetic barrier caused by magnetosheath reconnection gradually decreases the total pressures applied to the magnetopause thus resulting in the sunward magnetopause motion.

This paper builds upon the work of Samsonov et al. (2017) and investigates which parameters affect the magnetosheath propagation time. We will use MHD simulations with the solar wind conditions similar to the ones in Samsonov et al. (2017) but also simulated several artificial events and finally compare the numerical results with observed time delays in the ground response to solar wind DDs.

## 2. Flow Deceleration in the Magnetosheath

We use the Space Weather Modeling Framework global MHD model (Tóth et al., 2005, 2012) available through Community Coordinated Modeling Center (CCMC) runs on request to conduct our simulations. The grid spacing in the dayside magnetosheath was  $0.125 R_E$ .

For the solar wind input conditions, we use THEMIS B observations of the event on 7 August 2008 studied by Samsonov et al. (2017). We modify the original THEMIS data, shown in Figure 1, to keep all plasma parameters (i.e., density and velocity) constant and equal to values before the DD, leaving only the IMF  $B_y$  and  $B_z$  components to change. In this MHD run (called run 1 below), the solar wind density at the inflow boundary is  $3.26 \text{ cm}^{-3}$ ,  $V_x = -346 \text{ km/s}$ , and  $B_x = 0$ . We study the propagation of the DD with a southward turning marked by the red dashed line in Figure 1. Samsonov et al. (2017) found that the normal of the DD is directed along the Sun-Earth line, and it may be either a tangential or a rotational discontinuity.

We determine positions of the DD in the magnetosheath by two methods: first, using the maximum of the electric current density  $|j|$  ( $\mathbf{j} = (\nabla \times \mathbf{B})/\mu_0$ ) and second, finding the position where  $B_z = 0$  (since the IMF  $B_z$  changes from +3 to  $-2 \text{ nT}$  at the DD front). Both methods give almost the same results with an accuracy limited only by the finite spatial resolution. We also use three different methods to find the subsolar magnetopause: first, as the maximum in  $|j|$ , second, as the boundary between open and closed field line topologies, and third, using the condition  $V_x = 0$ . Again, the three methods give nearly identical values limited mainly by the grid resolution. We illustrate results of these methods and discuss the role of spatial resolution in Appendix A. The bow shock position is given only by a maximum in  $|j|$ .

Figure 2a shows simulation predictions for variations of the magnetopause, DD, and bow shock positions during the 15-min interval in which the DD crosses the magnetosheath. The magnetopause position varies only slightly, moving on average  $0.2 R_E$  sunward during the interval. The bow shock position almost does not change, and the DD crosses the magnetosheath with a gradually decreasing speed. Both the sunward magnetopause motion and the DD deceleration near the magnetopause confirm the previous results of Samsonov et al. (2017). The DD imposed at the upstream numerical boundary ( $x = 32 R_E$ ) at 19:25 UT crosses the bow shock at 19:30 UT and reaches the magnetopause at  $\sim 19:44$  UT. As the DD speed falls to about 10–20 km/s at that time and the distance between the DD and magnetopause decreases to several hundred kilometers, we cannot determine exactly the time of interaction between the DD and magnetopause. The spatial scale

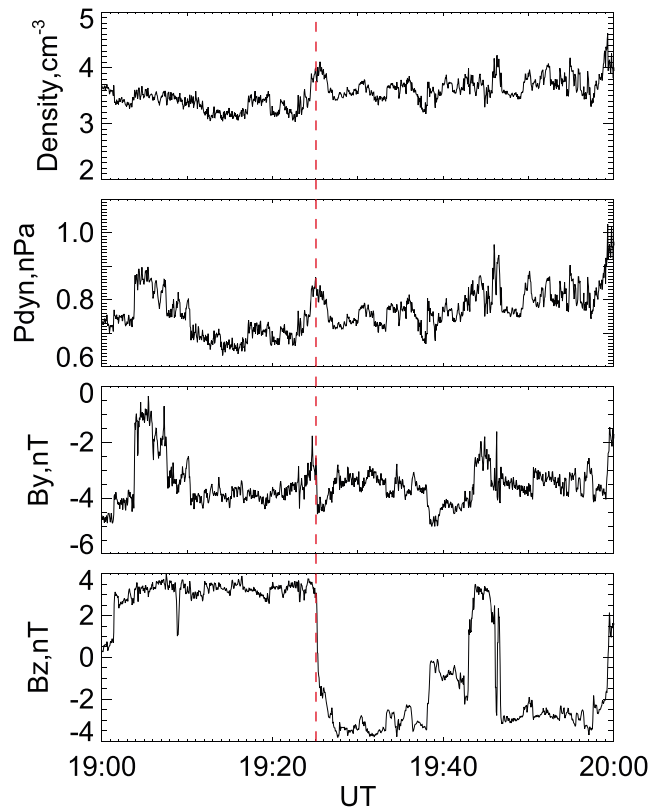


**Figure 1.** The solar wind density, dynamic pressure, IMF  $B_y$ , and  $B_z$  observed by THEMIS B. Dashed vertical line marks the southward turning at 19:25 UT.

becomes too small for a 3-D global MHD model and approaches the accuracy limit for MHD models. However, this time estimate agrees well with real ground and spacecraft observations, in particular, the polar cap index increases after 19:45 UT (Samsonov et al., 2017).

There is another way to find the DD propagation time between the subsolar bow shock and magnetopause. We assume that the DD propagates with the flow velocity. This is exactly correct for tangential discontinuities, while rotational discontinuities move with the Alfvén velocity with respect to plasma flow, that is, slightly faster than tangential discontinuities. Using the velocity profile along the Sun-Earth line at 19:30 UT, when the DD is slightly upstream from the bow shock, we calculate the positions of an imaginary particle moving

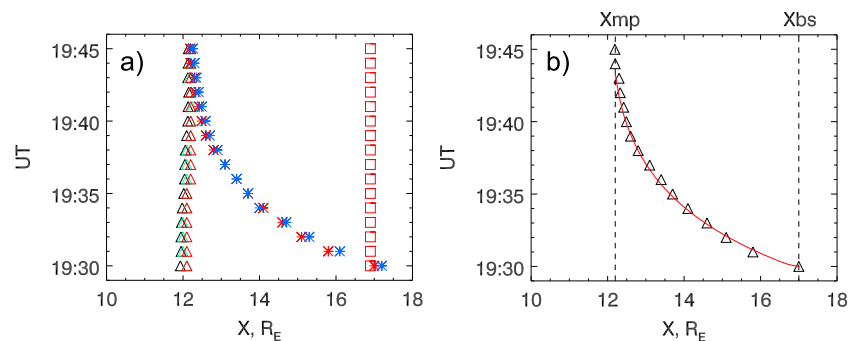


**Figure 2.** (a) Magnetopause (triangles), directional discontinuity (stars), and bow shock (squares) positions at the Sun-Earth line as functions of time. Red color indicates positions determined by maximal  $|j|$ , black triangles mark the magnetopause as the boundary between open and closed field lines, green triangles mark position  $V_x = 0$ , blue stars indicate the DDs determined from  $B_z = 0$ . (b) Positions of the DD determined by maximal  $|j|$  (black triangles) and calculated from the initial  $V_x$  profile (red line). Vertical dashed lines indicate magnetopause and bow shock positions. DD = directional discontinuity.

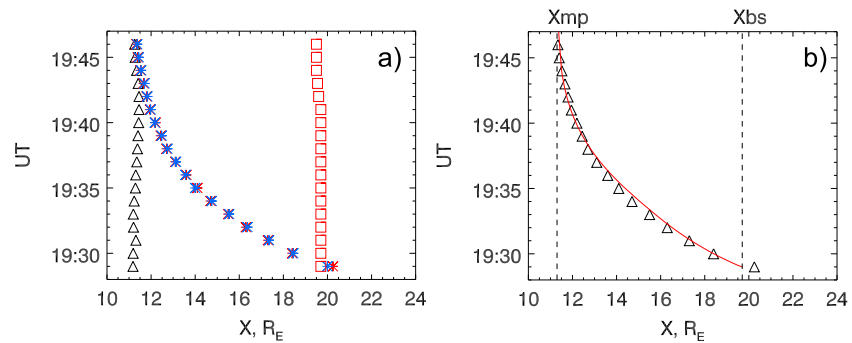


**Figure 3.** The same parameters as in Figure 2, but for a stronger IMF (the IMF  $B_z$  varies through the DD from +10 to  $-10$  nT; run 2). IMF = interplanetary magnetic field. DD = directional discontinuity.

with the flow speed. Figure 2b shows both the DD positions determined from maximal  $|j|$  (black triangles) and motion with the flow speed calculated from the quasi-stationary profile at 19:30 UT (red line). Both positions coincide with the accuracy limited by the grid resolution; thus, the DD moves with the same speed as the plasma flow, as expected for a tangential discontinuity.

We have made two other runs for DDs with different IMF magnitudes or solar wind speeds. In run 2, the plasma parameters were taken the same, but IMF  $B_z$  varied from +10 to  $-10$  nT. Thus, the solar wind Alfvén Mach number in run 2 was 2.7, that is, significantly lower than  $\sim 5.7$  in run 1. Figure 3 shows the DD propagation in this run. The magnetosheath width increases to  $8.5 R_E$  in comparison to  $4.8 R_E$  in run 1; however, the time required for the DD to cross the magnetosheath is only  $\sim 2$  min longer. The DD crosses the bow shock at 19:29 UT (1 min before the time in run 1) and reaches the magnetopause nearly at 19:45 UT (1 min later). We should mention again that the time for the magnetopause crossing cannot be determined exactly. We assume that the DD reaches the magnetopause when the distance between the two boundaries decreases to about one grid spacing. We will discuss this below.

In run 3 (not shown), we simulate a DD with the same variation in  $B_z$  as in run 1, but with a constant solar wind  $V_x$  equal to 800 km/s. The motion of the DD from the bow shock to the magnetopause is qualitatively the same as in runs 1–2 (motion with the plasma speed), but the magnetosheath width decreases to  $2.7 R_E$ , while the propagation time is only 6 min. Thus, a high solar wind speed significantly decreases the propagation time.

The discussion above shows that the magnetosheath propagation time of DD can be calculated using the initial (not disturbed by DD front) velocity profile along the Sun–Earth line. Below we discuss parameters that influence the propagation time delay.

### 3. Velocity Profiles at the Sun–Earth Line

Figure 4a shows  $V_x$  profiles along the Sun–Earth line for runs 1 and 2. The profiles were taken at 19:30 (run 1) and 19:27 (run 2) UT, before the DD crossed the bow shock. Small values for the solar wind  $V_y$  and  $V_z$  (17 and 18 km/s) do not play a role in the earthward motion of the DD. In run 1, the magnetopause and bow shock positions are at  $12.2$  and  $17.0 R_E$ . The solar wind speed decreases sharply across the bow shock, but then varies nearly linearly from a postshock value  $V_1$  to zero at the subsolar magnetopause. There is a thin layer with a small positive  $V_x$  just earthward of the magnetopause, and the speed remains very small in the dayside magnetosphere closer to the Earth.

In run 2 with a larger IMF magnitude, the velocity profile looks slightly different. The magnetopause and bow shock are located at  $11.2$  and  $19.7 R_E$ ; therefore, the magnetosheath thickness is  $3.7 R_E$  larger than in run 1. The postshock value ( $V_1$ ) is greater, and  $V_x$  does not change linearly through the magnetosheath: the gradient is stronger near the magnetopause. The thermal and magnetic pressure profiles along the Sun–Earth line (not shown) in run 2 differ both quantitatively and even qualitatively from those in run 1, but a detailed study of the effects of strong IMF (for low plasma beta) on the magnetosheath parameters lies outside the scope of the present work.

Quasi-linear dependences of  $V_x$  on  $x$  between the subsolar magnetopause and bow shock have been seen in other MHD simulations (e.g., Erkaev et al., 1999; Samsonov & Pudovkin, 2000; Wang et al., 2004; Wu, 1992).

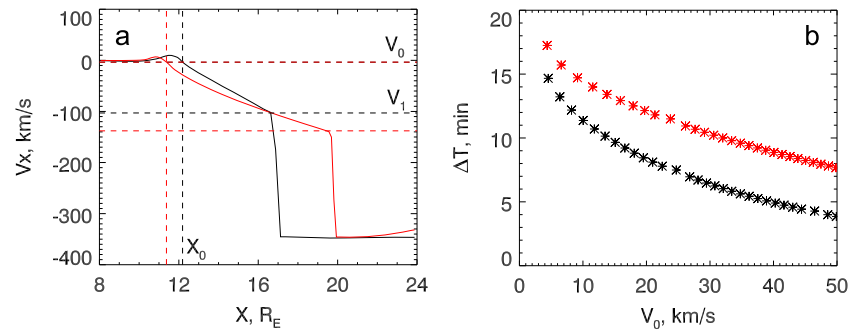


**Figure 4.** (a) Velocity profiles along the Sun–Earth line before the DD interaction with the bow shock in runs 1 (black) and 2 (red).  $V_0$  and  $X_0$  indicate the cutoff velocity and the corresponding coordinate near the magnetopause (see details in text).  $V_1$  indicates the velocity downstream of the bow shock. (b) The magnetosheath propagation time as a function of the cutoff velocity calculated from the velocity profiles in runs 1 (black) and 2 (red).

According to the pioneering magnetosheath simulation (Spreiter et al., 1966), the stagnation point with  $V = 0$  occurs at the subsolar magnetopause. Below, we estimate the magnetosheath propagation time considering an ideal velocity profile with a linear speed decrease from  $V_1$  just downstream from the bow shock to  $V_0$  very close to the magnetopause.

We integrate the velocity profile

$$T = \int_{X_{BS}}^{X_{MP}} \frac{dx}{|V_x|} = (X_{BS} - X_{MP}) \int_0^1 \frac{d\alpha}{V_0(1 - \alpha) + V_1\alpha}, \quad (1)$$

where  $T$  is the magnetosheath propagation time,  $X_{BS}$  and  $X_{MP}$  are bow shock and magnetopause coordinates, and  $\alpha = (X - X_{MP}) / (X_{BS} - X_{MP})$ . Then we get

$$T = \frac{(X_{BS} - X_{MP})}{(V_1 - V_0)} \int_0^{V_1 - V_0} \frac{d\alpha'}{\alpha' + V_0} = \frac{(X_{BS} - X_{MP})}{(V_1 - V_0)} \ln \frac{V_1}{V_0}. \quad (2)$$

Assuming a linear  $V_x$  profile, we find that  $T$  depends only on the magnetosheath thickness, postshock, and cutoff velocities ( $V_1$  and  $V_0$ ). The magnetosheath thickness and  $V_1$  can be calculated from the upstream solar wind parameters. The cutoff speed  $V_0$  does not have a straightforward definition. In MHD theory,  $V_0$  for a southward IMF case can be obtained from the reconnection velocity (estimated as  $\sim 0.1 V_A$ , where  $V_A$  is Alfvén speed near the subsolar magnetopause), but  $V_0 = 0$  for a northward case when reconnection occurs behind the cusps. However, substituting  $V_0 = 0$  gives infinite propagation times in (2). This is a stationary MHD solution, but in reality the magnetopause is always in motion with a typical speed of about 10–20 km/s (e.g., Kaufmann & Konradi, 1973; Paschmann et al., 1993; Phan & Paschmann, 1996). According to Paschmann et al. (1993), the normal magnetopause speed even in low magnetic shear cases does not fall below 3 km/s. Using the velocity profiles in runs 1 and 2 in Figure 2a, we calculate the magnetosheath propagation times as functions of  $V_0$ . Figure 4b shows these results.

Each star in Figure 4b corresponds to a grid point in the magnetosheath with  $V_0$  between 4 and 50 km/s. The corresponding propagation times vary between 4 and 14.7 min in run 1, and between 8 and 17.2 min in run 2. The smallest velocity corresponds to the grid point closest to the magnetopause. Assuming  $V_0 = 10$  km/s, we get 11.4 and  $\sim 14.4$  min in runs 1 and 2, respectively. The propagation times obtained for  $V_0$  between 4 and 10 km/s agree better with both previous observations cited by Samsonov et al. (2017) and the data analysis in section 5.

There are two limitations in the numerical MHD simulations. The first is the finite spatial resolution: the grid spacing in the subsolar magnetosheath was  $\sim 800$  km in these particular runs. The second is the intrinsic limitations of the MHD approach, for example, that the spatial scale must be larger than the proton gyroradius. The latter distance is about 1 order of magnitude smaller near the magnetopause than the grid spacing. By higher-resolution grids, we could possibly decrease  $V_0$  and increase the propagation time. However, it does not make much sense because the propagation times in the presented simulations agree well with the observed time delays discussed in section 5.

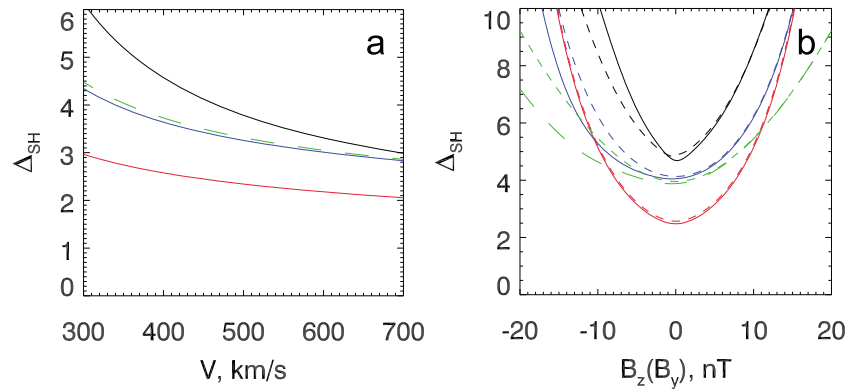


**Figure 5.** (a) Subsolar magnetosheath thickness as a function of the solar wind speed (black line = Ch02 model; blue = FR94 model; long-dashed green = CG94 model; red = J05 model). (b) Magnetosheath thickness as functions of IMF  $B_z$  (solid lines) and  $B_y$  (dashed lines) for the same models. Magnetosheath thickness as functions of IMF  $B_z$  for CG94 model shown by the long-dashed green line. IMF = interplanetary magnetic field.

#### 4. Propagation Time as a Function of Solar Wind Parameters

According to (2), the magnetosheath propagation time depends on  $V_0$ ,  $V_1$ , and the magnetosheath thickness  $\Delta_{SH}$  (distance between the subsolar bow shock and magnetopause). In turn, both  $V_1$  and  $\Delta_{SH}$  depend on solar wind parameters. Immediately downstream of the bow shock nose,  $V_1$  is the solar wind speed divided by the compression ratio through the bow shock, and the compression ratio can be expressed in terms of the solar wind Mach number (Spreiter et al., 1966)

$$V_1 = V_{SW} \frac{\rho_{SW}}{\rho_1} = V_{SW} \frac{(\gamma - 1)M_f^2 + 2}{(\gamma + 1)M_f^2}. \quad (3)$$

Here  $V_{SW}$  is the solar wind speed,  $M_f$  is the fast magnetosonic Mach number (see comments on Mach numbers in Formisano et al., 1971), and  $\gamma$  is the ratio of specific heats.

The magnetosheath thickness can be estimated using rather semiempirical expressions or empirical bow shock and magnetopause models. Using aerodynamic results, Spreiter et al. (1966) suggested an empirical expression related to (3)

$$\Delta_{SH} = 1.1X_{MP} \frac{(\gamma - 1)M_f^2 + 2}{(\gamma + 1)M_f^2}. \quad (4)$$

However, it follows that  $\Delta_{SH} = 1.1X_{MP}$  for  $M_f = 1$  while the physically correct behavior is  $\Delta_{SH} \rightarrow \infty$ . Therefore, Farris & Russell, 1994 (1994, FR94) suggested a correction of (4) important for small  $M_f$

$$\Delta_{SH} = 1.1X_{MP} \frac{(\gamma - 1)M_f^2 + 2}{(\gamma + 1)(M_f^2 - 1)}. \quad (5)$$

Cairns & Grabbe, 1994 (1994, CG94), also using Spreiter et al., 1966's (1966) relation between the shock jump condition and the magnetosheath thickness, suggested other expressions for  $\Delta_{SH}$  that predict nearly the same bow shock positions as FR94 model for typical solar wind conditions, but differ from FR94 model for stronger than usual IMF magnitudes.

Using spacecraft observations, a number of empirical magnetopause and bow shock models have been developed. In addition to the FR94 and CG94 models, we calculate  $\Delta_{SH}$  using recent bow shock models of Chao et al., 2002 (2002, Ch02) and Jeráb et al., 2005 (2005, J05), and Shue et al. (1998)'s model for position of the subsolar magnetopause.

We assume that the magnetosheath propagation time depends mainly on the solar wind speed and IMF magnitude and direction. The influence of the solar wind density and temperature on the magnetosheath thickness,  $V_0$  and  $V_1$  is supposed to be less significant. Figure 5 shows the magnetosheath thickness as a function of the solar wind speed and IMF  $B_z$  (and  $B_y$ ) magnitude using the Ch02 (black), FR94 (blue), and J05 (red) models with  $\gamma = 5/3$ .

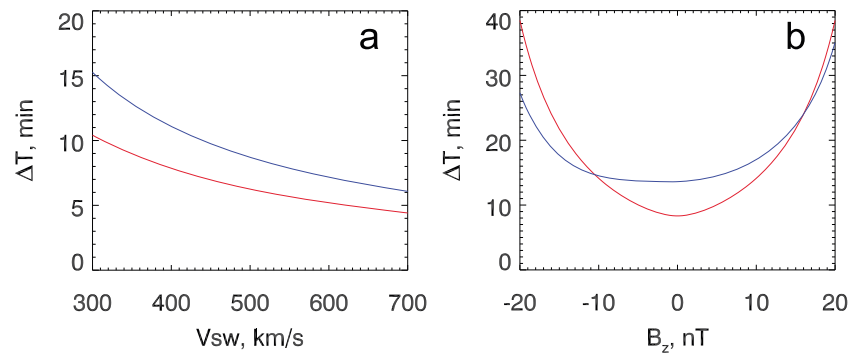


**Figure 6.** (a) Magnetosheath propagation time as a function of the solar wind speed (blue = FR94 model; red = J05 model). (b) Magnetosheath propagation time as a function of interplanetary magnetic field  $B_z$  for the same models.

We use Shue et al., 1998's (1998) model to obtain the position of the subsolar magnetopause in the FR94, CG94, and Ch02 models, while the magnetopause distance was calculated from the pressure balance in the J05 model. Using the J05 bow shock model in combination with the Shue et al., 1998's (1998) magnetopause model gives the same dependence qualitatively but the magnetosheath thickness diminishes by about 1.5  $R_E$ , because the J05 model tends to underestimate the standoff position of the subsolar bow shock. Recent studies show that Shue et al., 1998's (1998) model overestimates the radial distance to the high-latitude magnetopause (Case & Wild, 2013) but slightly underestimates the radial distance to the subsolar point (Samsonov et al., 2016). We employ the Shue et al. (1998) model because it is simple, widely used throughout the scientific community, and qualitatively reproduces known dependences on solar wind parameters quite well.

We should mention that several analytical models for the magnetosheath plasma flow and/or magnetic field have been developed (Génot et al., 2011; Kobel & Flückiger, 1994; Romashets et al., 2008; Soucek & Escoubet, 2012), which provide quasi-stationary solutions using predetermined magnetopause and bow shock shapes. We do not use these models here because we study a nonstationary problem and obtain velocity and magnetic field distributions in the magnetosheath from global MHD simulations.

We do not intend to compare the accuracy of the different models in this paper (e.g., using higher  $\gamma$  may improve predictions in some bow shock models) but only want to illustrate the fact that the dependences of  $\Delta_{SH}$  on  $V_{SW}$ ,  $B_z$ , and  $B_y$  are similar for all models. The magnetosheath thickness decreases as  $V_{SW}$  increases and increases as the magnitudes of both  $B_z$  and  $B_y$  increase. This agrees with expectation based on previous numerical studies (Farrugia et al., 1995). Since the models predict very similar dependencies on  $B_z$  and  $B_y$  (except differences caused by large negative  $B_z$ ), it seems that the magnitude of the IMF in the Y-Z plane is more important than the IMF orientation for  $\Delta_{SH}$ .

Figure 6 shows the magnetosheath propagation time calculated from (2) as a function of the solar wind speed and IMF  $B_z$  for the FR94 and J05 models. We vary only one selected solar wind parameter and keep others constant. The value for  $V_1$  is obtained from (3), and  $V_0 = 5$  km/s. Note that varying  $V_{SW}$  we take  $N_{SW} = 3.3$  cm $^{-3}$ ,  $B_x = 0$  nT,  $B_y = -2.6$  nT, and  $B_z = 3.1$  nT, while varying  $B_z$  we take  $V_{SW} = 346$  km/s consistent with the solar wind parameters upstream of the DD on 7 August 2008. For the given parameters, the magnetosheath propagation time varies between 4 and 15 min for solar wind speeds between 300 and 700 km/s. If  $|B_z|$  (or  $|B_y|$ ) is less than 10 nT, variations of the IMF magnitude slightly change the propagation time (by no more than several minutes). However, for a strong IMF  $|B| > 10$  nT (and a relatively low speed as mentioned above) the propagation time significantly increases and may exceed 30 min.

Another way to calculate the magnetosheath propagation time is to use the velocity profile along the Sun-Earth line obtained from MHD simulations. We have made two simulation runs varying either solar wind  $V_x$  or  $B_z$  and keeping constant all other parameters. We change  $V_x$  or  $B_z$  in a step-like function and then keep constant all solar wind parameters throughout a half-hour interval until a new quasi-stationary solution is obtained. We use velocity profiles so obtained to calculate the propagation time.

Figure 7 shows the velocity profiles along the Sun-Earth line for  $V_x = 300, 450,$  and  $600$  km/s (with  $B_y = 2$  and  $B_z = 4$  nT), and  $B_z = -20, -10, 0, 10,$  and  $20$  nT (with  $V_x = -400$  km/s), as obtained from the global MHD simulation. For typical IMF conditions,  $V_x$  varies nearly linearly between the magnetopause and bow

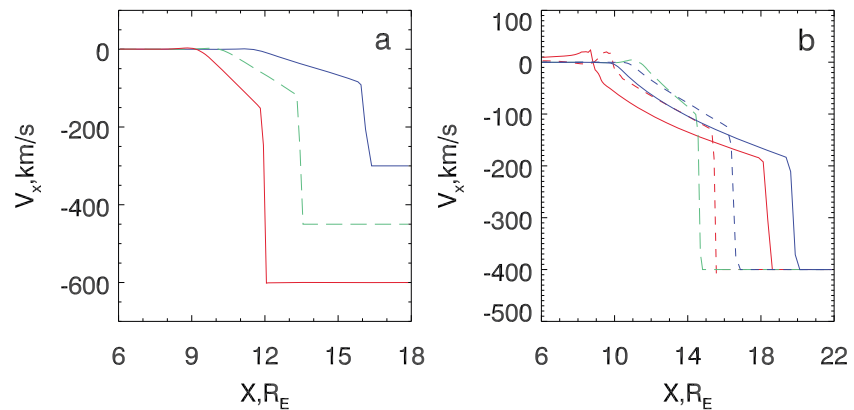


**Figure 7.** (a) Velocity profiles along the Sun-Earth line for  $V_{SW} = 300$  (blue),  $450$  (long-dashed green), and  $600$  (red) km/s (with  $B_z = 4$  nT). (b) Velocity profiles for  $B_z = -20$  (red solid),  $-10$  (red dashed),  $0$  (long-dashed green),  $10$  (blue dashed), and  $20$  (blue solid) nT (with  $V_{SW} = 400$  km/s).

shock as noted above. But for  $B_z = -20, -10,$  and  $20$  nT, it becomes clear that the speed decreases faster near the magnetopause, which is probably related to the stronger magnetic field. From Figure 7b, we can infer that  $V_0$  is larger for southward IMF, and there is a sunward flow in the outer magnetosphere possibly related to the global magnetospheric convection. The magnetosheath thickness increases with decreases of  $V_x$  and increases of  $|B_z|$  as mentioned above.

Figure 8 shows the magnetosheath thickness and propagation times as functions of the solar wind speed and  $B_z$ , as obtained from the MHD models. Triangles indicate results obtained directly from the velocity profiles in the MHD simulations, solid lines are calculated from (2) with  $V_0 = 5$  km/s (taking the same simulated magnetosheath thickness), and the dashed line is calculated from (2) but for  $V_0 = 20$  km/s. In the simulation, we take the cutoff velocity at a point near to, but greater than 5 km/s. As we show below, this method to determine the cutoff velocity results in a large scatter of  $V_0$  for different velocity profiles. This is a consequence of the finite spatial resolution; therefore,  $V_0$  may vary between 5 and 20 km/s. The scatter in  $V_0$  results in the scatter in the propagation times obtained from the velocity profiles (triangles in Figures 8c and 8d), especially for southward IMF because the  $|V_x|$  gradient may increase sharply near the magnetopause in this case.

The results in Figures 8a and 8b are qualitatively similar to the results in Figure 5 and show a decrease in the magnetosheath thickness from  $4.2$  to  $2.3 R_E$  as  $V_x$  increases from  $300$  to  $700$  km/s. Figure 8b shows that  $\Delta_{SH}$  increases from  $3.0$  to  $9.5$  ( $9.6$ )  $R_E$  for  $B_z$  varying from  $0$  to  $-20$  ( $+20$ ) nT. Correspondingly, the magnetosheath propagation time decreases from  $16.2$  to  $6.7$  min as the solar wind velocity increases. Figure 8d shows that the propagation time is smallest ( $7.7$  min) for  $B_z = -4$  nT and increases to  $12.6$  min for  $B_z = -20$  nT and to  $18.0$  min for  $B_z = 20$  nT. Thus, the two different methods in Figures 6 and 8 consistently predict that propagation times increase with decreasing  $V_x$  and increasing  $|B_z|$ . Some quantitative differences are related to differences in other solar wind parameters (e.g., the solar wind speed is higher for the simulations in Figure 8d than in Figure 6b).

This section discussed parameters that determine magnetosheath propagation times. Increases in the solar wind flow speed result in increases in the average magnetosheath flow speed and decreases in the magnetosheath thickness. Both factors lead to decreases in the propagation time. Increases in the magnetic field magnitude ( $|B_z|$  in our case) result in increases in the magnetosheath thickness and corresponding increases in the propagation time.

## 5. Timing the Response to Directional Discontinuities Seen in Ground Observations

To confirm our numerical predictions, we now consider observations defining the response to solar wind DD seen in ground data. We have chosen 35 events with both northward and southward IMF turnings observed by the Time History of Events and Macroscale Interactions during Substorms (THEMIS) spacecraft, probes THEMIS B and THEMIS C, in the solar wind about  $10$ – $15 R_E$  upstream of the bow shock. We select events with steady  $B_z$  during  $15$ – $20$  min before and  $\geq 5$  min after the passage of the discontinuity front. The duration of

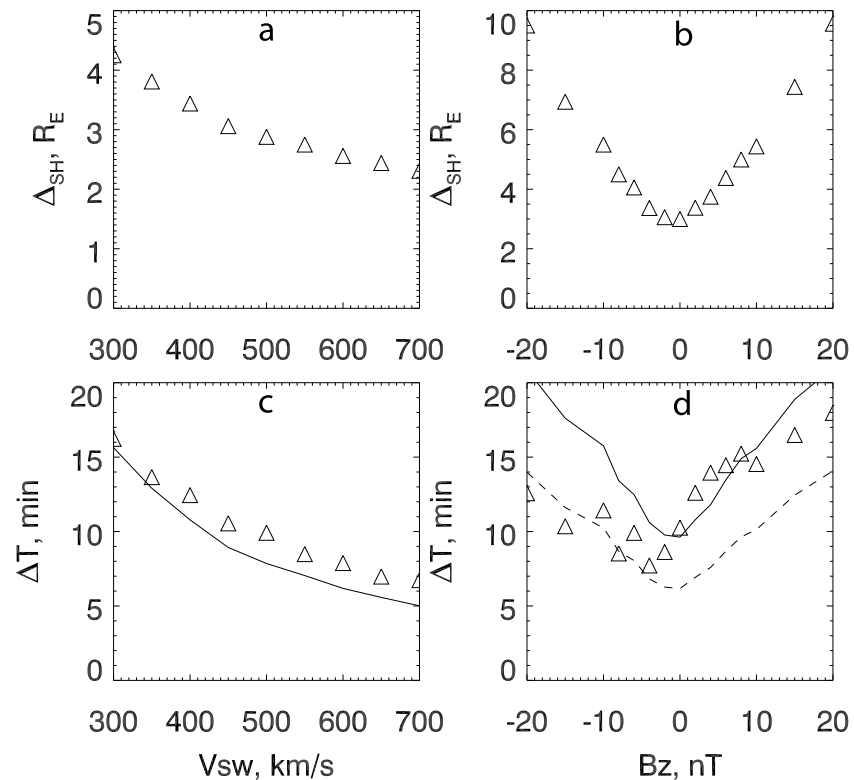


**Figure 8.** The magnetosheath thickness (top panels) and propagation times (bottom) as functions of the solar wind speed and interplanetary magnetic field  $B_z$ . Triangles indicate results obtained directly from the velocity profiles, the solid lines are calculated from (2) with  $V_0 = 5$  km/s, the dashed line is also calculated from (2) but for  $V_0 = 20$  km/s. (left) Dependence on the solar wind speed with  $B_z = 4$  nT, (right) dependence on the IMF  $B_z$  with  $V_{sw} = 400$  km/s.

the discontinuities must not exceed 2 min, and the jump of  $B_z$  must exceed 2 nT. The geomagnetic activity in all events was low, that is, without magnetic storms or strong substorms.

The time of the ground response has been determined from variations in the PCN index: the PCN index increases in response to southward IMF turnings and decreases in response to northward turnings. We calculate the time delays of the ground response relative to the time when the DD should interact with the subsolar bow shock. We take into account the positions of THEMIS and the orientations of the DD fronts. We exclude very tilted DD fronts from our database. The angle between the DD normal and the Sun-Earth line is less than  $45^\circ$  for 60% of the DDs, and the angles for the rest lie between  $45$  and  $61^\circ$ .

Figure 9 shows the time delays as a function of the solar wind speed. The red line represents an exponential fit to all points. In general, the observations confirm that the time delay decreases with increases in the solar wind speed. Moreover, the results in Figure 9 quantitatively agree with the simulation results shown in Figure 8. In particular, as indicated by the red line, the time delay of 15 min corresponds to the speed of 300 km/s, while 7 min corresponds to 600 km/s. The numerical results for the magnetosheath propagation time in Figure 8 give nearly the same values. Note that Figures 8 and 9 actually show different times, the first is the magnetosheath propagation time, and the second is the time delay of the ground response. However, we follow the suggestion of Samsonov et al. (2017) that the time interval from the DD interaction with the magnetopause to the first ground response is small (only about 1–2 min). This time is related to the time of propagation of Alfvén wave from the magnetopause to the ionosphere, which is about 1 min.

Despite the good agreement between the observed time delays and simulation results, the scatter in Figure 9 is very large. We explain this by two factors. First, as noted above, the solar wind speed is not the only parameter that determines the magnetosheath propagation time. As we have noted, another parameter is the IMF magnitude. Second, we have shown that variations in the near-magnetopause cutoff speed  $V_0$  may change the propagation time and we have no reliable method to take this effect into account now.

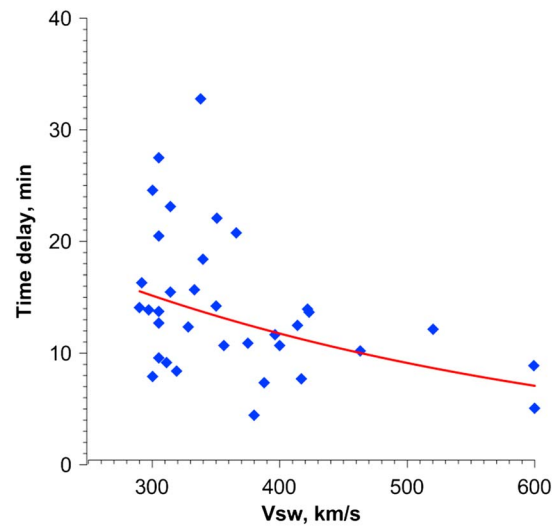


**Figure 9.** Time delays of ground response to both southward and northward interplanetary magnetic field turnings counted from the contact of directional discontinuities with the subsolar bow shock. The red line represents the least squares fit.

The average time delay obtained for all DDs in Figure 9 is 12.8 min. The DDs with northward turnings show an average delay of 11.8 min, while the DDs with southward turnings show an average delay of 13.9 min. The northward turnings correspond to initial southward IMF conditions; therefore, time delays in such events may be smaller because of larger  $V_0$ . Taking into account the large scatter in the observed time delays, the difference about 2 min between the average northward and southward delays is nearly insignificant; however, it agrees with the MHD simulations in Figure 8d, which show larger propagation times through the magnetosheath for quasi-stationary velocity profiles during northward IMF intervals.

## 6. Discussion and Conclusions

We studied the interaction of solar wind directional (both tangential or rotational) discontinuities with the Earth's magnetosphere. Previous observations indicated delays in the ground (ionospheric) response to discontinuities with southward or northward turnings. We found that the average time delay from the contact of DD with the subsolar bow shock to the ground response is 13 min. Although there is a large scatter, this estimate agrees with previous results. The time delays in our statistics vary from 4.5 to 33 min mainly due to different solar wind conditions.

Recently, Samsonov et al. (2017) considered an event with a southward IMF turning on 7 August 2008 and explained the observed time delay in the ground response in terms of a large magnetosheath propagation time. Using global MHD simulations, they showed that it took about 14 min for the solar wind DD to cross the subsolar magnetosheath. Samsonov et al. (2017) noted that a steady northward IMF before the DD results in the formation of the magnetic barrier near the magnetopause and this magnetic barrier must be completely destroyed by magnetic reconnection at the DD front before the discontinuity can reach the magnetopause. High-speed reconnection jets in the magnetosheath originating at narrowing DD current layers were previously simulated and observed by Maynard et al., 2002 (2002, 2007) and Phan et al. (2007). However, the magnetic barrier may be evacuated from the subsolar region both by magnetic reconnection and by accelerated flows in front of the magnetopause in the direction perpendicular to magnetic field lines. We checked the latter assumption in Appendix B.

This paper continues the study of Samsonov et al. (2017) by investigating which parameters influence the propagation times of solar wind DDs traversing the magnetosheath. We first show that the DD moves through the magnetosheath with the flow velocity in MHD simulations. Therefore, we can find magnetosheath propagation times by integrating speeds from the bow shock to the magnetopause. Expression (2) contains three parameters that determine the propagation time, they are the magnetosheath thickness  $\Delta_{SH}$ , the speed immediately downstream of the bow shock  $V_1$ , and the speed immediately upstream of the magnetopause  $V_0$ .

Both  $\Delta_{SH}$  and  $V_1$  depend on solar wind conditions. We select two solar wind parameters, the solar wind speed and IMF  $B_z$ , which should have strong effects on propagation times. Indeed, the simulations show that the propagation time increases from about 5 to 16 min when the speed decreases from 700 to 300 km/s. Nearly the same values were obtained from observations of the ground response shown in Figure 9.

Although we consider only IMF  $B_z$  in detail, we believe that the IMF magnitude in the Y-Z plane rather than the sign of  $B_z$  is the most important factor. Larger IMF magnitudes result in larger magnetosheath thicknesses, and as a result in larger propagation times. Our results suggest that the IMF magnitude significantly influences the propagation time for a strong magnetic field, for example, for  $|B| > 10$  nT. The MHD simulation shows that the sign of  $B_z$  may also influence the propagation time. The propagation time is somewhat shorter for a southward IMF (prior to the DD) than for a northward IMF with the same magnitude. We suggest that this effect comes into play via another parameter  $V_0$ , the speed at the subsolar magnetopause.

If the magnetopause is a tangential discontinuity, hydrodynamic and MHD solutions (e.g., Spreiter et al., 1966) predict a stagnation point in the subsolar region where the speed falls to zero. However, magnetopause reconnection may result in plasma penetration through the dayside magnetopause and rapid acceleration of plasma and magnetic fields away from the subsolar point along the surface of the magnetopause. Moreover, the magnetopause usually moves with a speed of about 10–20 km/s, leading us to expect that the condition  $V = 0$  never occurs in the magnetosheath. For the given typical solar wind conditions, the propagation time decreases from 15 to 4 min as  $V_0$  increases from 4 to 50 km/s. Reasonable estimates for the propagation time suggest  $V_0$  about 5 km/s for northward IMF and about 20 km/s for southward IMF.

We compared  $V_x$  profiles along the Sun-Earth line in the MHD simulations for stationary northward and southward IMF conditions (not shown) and found that the average  $V_x$  through the subsolar magnetosheath is 129 km/s for northward IMF and 164 km/s for southward IMF. This agrees with the larger  $V_0$  and shorter propagation time for southward IMF mentioned above. The smaller average velocity for northward IMF can be explained by the fact that the magnetic field strength near the magnetopause is larger and the Ampère's force pushes plasma away from the subsolar region.

At the same time, we obtain a large scatter extracting the propagation time from the MHD simulations for southward IMF, while the difference between the average time delays for northward and southward IMFs obtained from observations ( $\sim 2$  min) is almost the same as the accuracy of the time delay determination. This prevents us from making any firm conclusions comparing positive and negative  $B_z$  cases, and we postpone a detailed physical explanation of  $V_0$  for the future.

Summarizing this paper, we emphasize that flow deceleration in the magnetosheath must be taken into account when estimating propagation times for solar wind structures from the Lagrangian point to the subsolar magnetopause. Assuming that the solar wind structures move with the solar wind speed through the magnetosheath up to the magnetopause may result in significant underestimations of the propagation time. We believe that the conclusions of our paper are valid not only for tangential discontinuities (with sharp changes of IMF orientation as shown above), but for all solar wind structures convected with the solar wind speed.

We summarize the most important points below.

- DDs decelerate in the magnetosheath, leading to delayed ground responses to their arrival.
- The average time delay from the contact of DD with the subsolar bow shock to the ground response is about 13 min.
- This time delay depends on the solar wind speed and IMF magnitude and slightly changes with the IMF  $B_z$  polarity, being slightly smaller for a strong negative  $B_z$  on the leading edge of DD.
- The principal factor determining the time delay is the velocity profile through the magnetosheath, that in turn is influenced by magnetopause reconnection.

## Appendix A: Differences in Magnetopause Locations

We have used three different methods to find the subsolar magnetopause: first, as the maximum in  $|j|$ , second, as the boundary between open and closed field line topologies (using CCMC intrinsic routines), and third, using the condition  $V_x = 0$ . To illustrate how these methods work, Figure A1 presents  $V_x$  and  $|j|$  profiles along the Sun-Earth line: (1) for northward and southward IMF, (2) for typical and strong IMF magnitudes. The figure

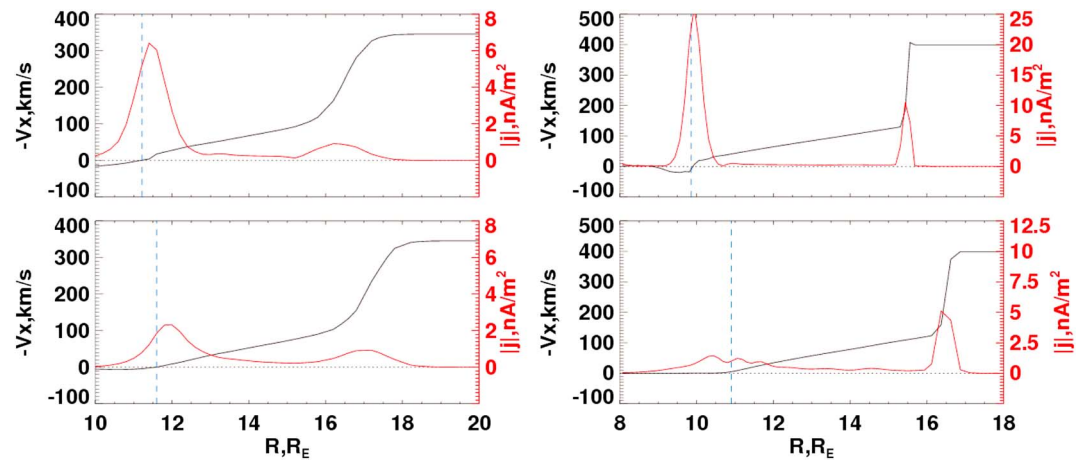


**Figure A1.** (left)  $V_x$  (black) and  $|j|$  (red) profiles along the Sun-Earth line for southward (top) and northward (bottom) IMF for typical solar wind parameters (conditions as in event 7 August 2008 before DD); (right) the same parameters in a strong IMF case ( $B_z = -10/+10$  nT). Vertical dashed lines indicate the boundary between open and closed field lines calculated for the CCMC runs. DD = directional discontinuity; IMF = interplanetary magnetic field; CCMC = Community Coordinated Modeling Center.

displays differences in magnetopause locations determined by the three methods and shows how these vary in response to IMF  $B_z$  sign and magnitude.

The figure demonstrates that (1) the open-closed field line boundary nearly coincides with the position where  $V_x = 0$  in all cases; (2) the location where  $|j|$  maximizes may be slightly farther from the Earth than the positions determined by the two other methods, but not by more than  $0.5 R_E$ ; that is, the difference is comparable to the grid resolution; (3) for a strongly northward IMF it can be difficult to determine the magnetopause position from the maximum in  $|j|$ , but we use  $V_x$  profiles to determine the magnetopause in such cases. Finally, the magnetopause lies closer to the Earth for southward IMF than for northward IMF, as expected when magnetopause reconnection is occurring.

To illustrate the effect of spatial resolution on magnetopause location, we compare results from two other runs with high ( $\Delta = 1/8 R_E$ ) and low ( $\Delta = 1/4 R_E$ ) resolutions for a strong southward IMF case. Figure A2 shows the corresponding  $V_x$  and  $|B|$  profiles in the both runs. Enhanced resolution results in (1) sharper magnetopause and bow shock discontinuities and (2) a slight decrease in the distance to the subsolar point which is possibly

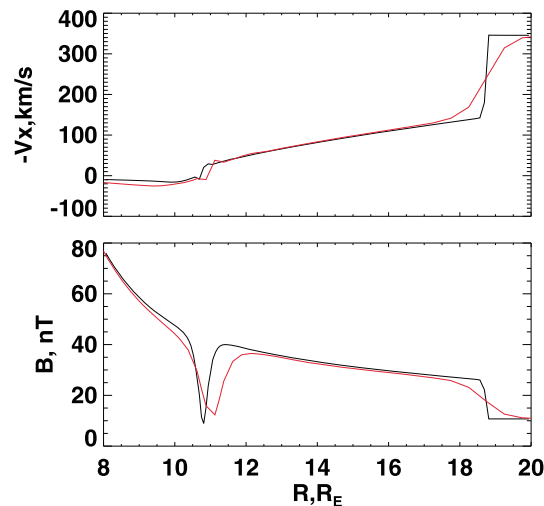


**Figure A2.** (top)  $-V_x$  and (bottom)  $|B|$  profiles along the Sun-Earth line in high (black) and low (red) spatial resolution runs for strong southward interplanetary magnetic field intervals.

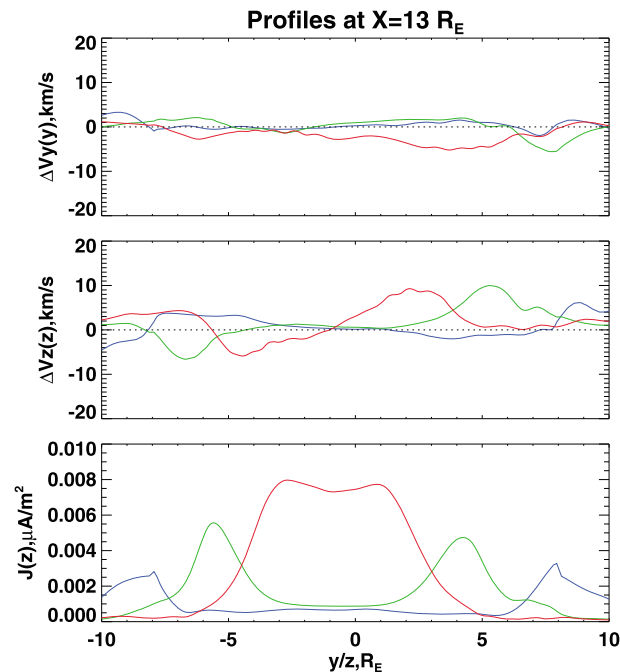


**Figure B1.** The differences in  $V_y(y)$  and  $V_z(z)$  profiles at 19:33 (blue), 19:35 (green), and 19:35 (red) UT with respect to initial  $V_y$  and  $V_z$  at 19:30 UT before the directional discontinuity crossing of the bow shock. The  $V_y(y)$  profile is along a straight line with  $x = 13R_E$  and  $z = 0$  (top), and the  $V_z(z)$  profile is along a line with  $x = 13R_E$  and  $y = 0$  (middle). At the Sun-Earth line, point  $x = 13R_E$  is only  $1R_E$  upstream of the magnetopause. The bottom panel shows the electric current density as a function of  $z$ .

related to the sharper discontinuity fronts. So we deduce that changes in spatial resolution do not change our conclusions.

In the same two runs, we compare velocity distributions in the noon-meridional plane (not shown). The flow velocity drops to nearly zero at the subsolar magnetopause and increases both northward and southward along the magnetopause finally exceeding the solar wind value. This is a signature of magnetopause reconnection. The velocity grows slightly faster in the high-resolution run.

## Appendix B: The Role of Magnetic Reconnection in Decay of the Magnetic Barrier

In this supplementary section we check whether the magnetic barrier in front of the magnetopause is destroyed mainly by magnetic reconnection at the DD front. If the magnetic barrier is removed by magnetic reconnection, the flow speed will increase in the direction along magnetic field, that is, along  $z$  axis. If the magnetic field lines upstream of the magnetopause are carried away solely by the accelerated magnetosheath flow, the velocity would increase mainly in the direction perpendicular to magnetic field (along  $y$  axis).

Figure B1 shows the differences in  $V_y(y)$ ,  $V_z(z)$ , and  $|j(z)|$  profiles about  $1R_E$  upstream of the subsolar magnetopause at 3 times during the DD motion through the magnetosheath. An increase in the electric current indicates the position of the DD front in the magnetosheath. The DD front reaches the subsolar magnetosheath at  $x = 13R_E$  nearly at 19:35 UT (red lines). The figure reveals an increase in  $V_z$  directed upward above and downward below the equatorial plane resulting from magnetic reconnection at the DD front. On the contrary,  $V_y$  changes insignificantly when the DD propagates through the magnetosheath. This result confirms our initial assumption that magnetic reconnection is the main mechanism to remove magnetic field pileup in front of the magnetopause.

## References

- Ardeéová, K. (2009). The study of instabilities in the solar wind and magnetosheath and their interaction with the Earth's magnetosphere. *Planetary and Space Science*, 57, 888–890. <https://doi.org/10.1016/j.pss.2008.12.005>
- Araki, T. (1994). A physical model of the geomagnetic sudden commencement. In M. J. Engebretson, K. Takahashi, & M. Scholer (Eds.), *Solar wind sources of magnetospheric ultra-low-frequency waves* (pp. 183–200). American Geophysical Union.

## Acknowledgments

This work was carried out using the SWMF/BATSRUS tools developed at the University of Michigan Center for Space Environment Modeling (CSEM) and made available through the NASA Community Coordinated Modeling Center (<http://ccmc.gsfc.nasa.gov>). We used results of the runs *Andrey\_Samsonov\_051817\_1*, *Andrey\_Samsonov\_100217\_2*, *Andrey\_Samsonov\_100417\_1*, *Andrey\_Samsonov\_111417\_1*, and *Andrey\_Samsonov\_111517\_1*. ACE, Wind, and THEMIS data are available from the Coordinated Data Analysis Web (CDAWeb), from the THEMIS mission site (<http://themis.ssl.berkeley.edu/>), and from ACE mission site (<http://www.srl.caltech.edu/ACE/>). The work of A. A. S. during his visit at NASA/GSFC was supported by the THEMIS mission. V. S. S. was supported by the Russian Science Foundation grant 18-47-05001. J. S. and Z. N. were supported by the Czech Science Foundation under contract 17-06065S.

- Bhaskar, A., & Vichare, G. (2013). Characteristics of penetration electric fields to the equatorial ionosphere during southward and northward IMF turnings. *Journal of Geophysical Research: Atmospheres*, *118*, 4696–4709. <https://doi.org/10.1002/jgra.50436>
- Cairns, I. H., & Grabbe, C. L. (1994). Towards an MHD model for the standoff distance to the Earth's bow shock. *Geophysical Research Letters*, *21*, 2781–2784. <https://doi.org/10.1029/94GL02551>
- Case, N. A., & Wild, J. A. (2013). The location of the Earth's magnetopause: A comparison of modeled position and in situ Cluster data. *Journal of Geophysical Research: Space Physics*, *118*, 6127–6135. <https://doi.org/10.1002/jgra.50572>
- Chao, J. K., Wu, D. J., Lin, C.-H., Yang, Y.-H., Wang, X. Y., Kessel, M., et al. (2002). Models for the size and shape of the Earth's magnetopause and bow shock. *COSPAR Colloquia Series*, *12*, 127–135. [https://doi.org/10.1016/S0964-2749\(02\)80212-8](https://doi.org/10.1016/S0964-2749(02)80212-8)
- Dungey, J. W. (1961). Interplanetary magnetic field and the auroral zones. *Physical Review Letters*, *6*, 47–48. <https://doi.org/10.1103/physrevlett.6.47>
- Erkaev, N. V., Farrugia, C. J., & Biernat, H. K. (1999). Three-dimensional, one-fluid, ideal MHD model of magnetosheath flow with anisotropic pressure. *Journal of Geophysical Research*, *104*, 6877–6887.
- Farris, M. H., & Russell, C. T. (1994). Determining the standoff distance of the bow shock: Mach number dependence and use of models. *Journal of Geophysical Research*, *99*(A9), 17,681–17,689. <https://doi.org/10.1029/94JA01020>
- Farrugia, C. J., Erkaev, N. V., Biernat, H. K., & Burlaga, L. F. (1995). Anomalous magnetosheath properties during Earth passage of an interplanetary magnetic cloud. *Journal of Geophysical Research*, *100*(A10), 19,245–19,257. <https://doi.org/10.1029/95JA01080>
- Formisano, V., Hedgcock, P. C., Moreno, G., Sear, J., & Bollea, D. (1971). Observations of Earth's bow shock for low Mach numbers. *Planetary and Space Science*, *19*, 1519–1531. [https://doi.org/10.1016/0032-0633\(71\)90011-0](https://doi.org/10.1016/0032-0633(71)90011-0)
- Génot, V., Broussillou, L., Budnik, E., Hellinger, P., Travníček, P. M., Lucek, E., & Dandouras, I. (2011). Timing mirror structures observed by Cluster with a magnetosheath flow model. *Annales Geophysicae*, *29*, 1849–1860. <https://doi.org/10.5194/angeo-29-1849-2011>
- Goncharov, O., Šafránková, J., & Němeček, Z. (2015). Interplanetary shock–bow shock interaction: Comparison of a global MHD model and observation. *Planetary and Space Science*, *115*, 4–11. <https://doi.org/10.1016/j.pss.2014.12.001>
- Hsu, T.-S., & McPherron, R. L. (2003). Occurrence frequencies of IMF triggered and nontriggered substorms. *Journal of Geophysical Research*, *108*(A7), 1307. <https://doi.org/10.1029/2002JA009442>
- Jeráb, M., Němeček, Z., Šafránková, J., Jelínek, K., & Merka, J. (2005). Improved bow shock model with dependence on the IMF strength. *Planetary and Space Science*, *53*, 85–93. <https://doi.org/10.1016/j.pss.2004.09.032>
- Kaufmann, R. L., & Konradi, A. (1973). Speed and thickness of the magnetopause. *Journal of Geophysical Research*, *78*(28), 6549–6568. <https://doi.org/10.1029/JA078i028p06549>
- Kobel, E., & Flückiger, E. O. (1994). A model of the steady state magnetic field in the magnetosheath. *Journal of Geophysical Research*, *99*, 23,617–23,622. <https://doi.org/10.1029/94JA01778>
- Kokubun, S., McPherron, R. L., & Russell, C. T. (1977). Triggering of substorms by solar wind discontinuities. *Journal of Geophysical Research*, *82*(1), 74–86. <https://doi.org/10.1029/JA082i001p00074>
- Koval, A., Šafránková, J., Němeček, Z., & Přeč, L. (2006). Propagation of interplanetary shocks through the solar wind and magnetosheath. *Advances in Space Research*, *38*(3), 552–558. <https://doi.org/10.1016/j.asr.2006.05.023>
- Koval, A., Šafránková, J., Němeček, Z., Přeč, L., Samsonov, A. A., & Richardson, J. D. (2005). Deformation of interplanetary shock fronts in the magnetosheath. *Geophysical Research Letters*, *32*, L15101. <https://doi.org/10.1029/2005GL023009>
- Koval, A., Šafránková, J., Němeček, Z., Samsonov, A. A., Přeč, L., & Richardson, J. D. (2006). Interplanetary shock in the magnetosheath: Comparison of experimental data with MHD modeling. *Geophysical Research Letters*, *33*, L1102. <https://doi.org/10.1029/2006GL025707>
- Maynard, N. C., Burke, W. J., Ober, D. M., Farrugia, C. J., Kucharek, H., Lester, M., et al. (2007). Interaction of the bow shock with a tangential discontinuity and solar wind density decrease: Observations of predicted fast mode waves and magnetosheath merging. *Journal of Geophysical Research*, *112*, A12219. <https://doi.org/10.1029/2007JA012293>
- Maynard, N. C., Sonnerup, B. U. Ö., Siscoe, G. L., Weimer, D. R., Siebert, K. D., Erickson, G. M., et al. (2002). Predictions of magnetosheath merging between IMF field lines of opposite polarity. *Journal of Geophysical Research*, *107*(A12), 1456. <https://doi.org/10.1029/2002JA009289>
- Nishida, A. (1978). *Geomagnetic diagnosis of the magnetosphere* (256 pp.). New York: Springer-Verlag. <https://doi.org/10.1007/978-3-642-86825-2>
- Oliveira, D. M., & Samsonov, A. A. (2017). Geoeffectiveness of interplanetary shocks controlled by impact angles: A review. *Advances in Space Research*, *61*(1), 1–44. <https://doi.org/10.1016/j.asr.2017.10.006>
- Paschmann, G., Baumjohann, W., Sckopke, N., Phan, T.-D., & Lühr, H. (1993). Structure of the dayside magnetopause for low magnetic shear. *Journal of Geophysical Research*, *98*, 13,409–13,422. <https://doi.org/10.1029/93JA00646>
- Phan, T. D., & Paschmann, G. (1996). Low-latitude dayside magnetopause and boundary layer for high magnetic shear: 1. Structure and motion. *Journal of Geophysical Research*, *101*(A4), 7801–7815. <https://doi.org/10.1029/95JA03752>
- Phan, T. D., Paschmann, G., Twitty, C., Mozer, F. S., Gosling, J. T., Eastwood, J. P., et al. (2007). Evidence for magnetic reconnection initiated in the magnetosheath. *Geophysical Research Letters*, *34*, L14104. <https://doi.org/10.1029/2007GL030343>
- Pudovkin, M. I. (1987). Formation and characteristics of the magnetic barrier in front of the dayside magnetopause. *Geomagnetizm i Aeronomiya*, *27*, 18–21.
- Ridley, A. J., Lu, G., Clauer, C. R., & Papitashvili, V. O. (1998). A statistical study of the ionospheric convection response to changing interplanetary magnetic field conditions using the assimilative mapping of ionospheric electrodynamics technique. *Journal of Geophysical Research*, *103*, 4023–4040. <https://doi.org/10.1029/97JA03328>
- Romashets, E. P., Poedts, S., & Vandas, M. (2008). Modeling of the magnetic field in the magnetosheath region. *Journal of Geophysical Research*, *113*, A02203. <https://doi.org/10.1029/2006JA012072>
- Ruohoniemi, J. M., & Greenwald, R. A. (1998). The response of high-latitude convection to a sudden southward IMF turning. *Geophysical Research Letters*, *25*, 2913–2916. <https://doi.org/10.1029/98GL02212>
- Samsonov, A. A., Gordeev, E., Tsyganenko, N. A., Šafránková, J., Němeček, Z., Šimůnek, J., et al. (2016). Do we know the actual magnetopause position for typical solar wind conditions? *Journal of Geophysical Research: Space Physics*, *121*, 6493–6508. <https://doi.org/10.1002/2016JA022471>
- Samsonov, A. A., Němeček, Z., & Šafránková, J. (2006). Numerical MHD modeling of propagation of interplanetary shock through the magnetosheath. *Journal of Geophysical Research*, *111*, A08210. <https://doi.org/10.1029/2005JA011537>
- Samsonov, A. A., & Pudovkin, M. I. (2000). Application of the bounded anisotropy model for the dayside magnetosheath. *Journal of Geophysical Research*, *105*(A6), 12,859–12,867. <https://doi.org/10.1029/2000JA900009>
- Samsonov, A. A., Sergeev, V. A., Kuznetsova, M. M., & Sibeck, D. G. (2015). Asymmetric magnetospheric compressions and expansions in response to impact of inclined interplanetary shock. *Geophysical Research Letters*, *42*, 4716–4722. <https://doi.org/10.1002/2015GL064294>
- Samsonov, A. A., Sibeck, D. G., Dmitrieva, N. P., & Semenov, V. S. (2017). What happens before a southward IMF turning reaches the magnetopause? *Geophysical Research Letters*, *44*, 9159–9166. <https://doi.org/10.1002/2017GL075020>

- Samsonov, A. A., Sibeck, D. G., & Imber, J. (2007). MHD simulation for the interaction of an interplanetary shock with the Earth's magnetosphere. *Journal of Geophysical Research*, *112*, A12220. <https://doi.org/10.1029/2007JA012627>
- Saunders, M. A., Freeman, M. P., Southwood, D. J., Cowley, S. W., Lockwood, M., Samson, J. C., et al. (1992). Dayside ionospheric convection changes in response to long-period interplanetary magnetic field oscillations—Determination of the ionospheric phase velocity. *Journal of Geophysical Research*, *97*, 19,373–19,380. <https://doi.org/10.1029/92JA01383>
- Shue, J.-H., Song, P., Russell, C. T., Steinberg, J. T., Chao, J. K., Zastenker, G., et al. (1998). Magnetopause location under extreme solar wind conditions. *Journal of Geophysical Research*, *103*, 17,691–17,700. <https://doi.org/10.1029/98JA01103>
- Smith, E. J. (1973). Identification of interplanetary tangential and rotational discontinuities. *Journal of Geophysical Research*, *78*(13), 2054–2063. <https://doi.org/10.1029/JA078i013p02054>
- Soucek, J., & Escoubet, C. P. (2012). Predictive model of magnetosheath plasma flow and its validation against Cluster and THEMIS data. *Annales Geophysicae*, *30*, 973–982. <https://doi.org/10.5194/angeo-30-973-2012>
- Spreiter, J. R., Summers, A. L., & Alksne, A. Y. (1966). Hydromagnetic flow around the magnetosphere. *Planetary and Space Science*, *14*, 223–253. [https://doi.org/10.1016/0032-0633\(66\)90124-3](https://doi.org/10.1016/0032-0633(66)90124-3)
- Taylor, J. R., Cowley, S. W. H., Yeoman, T. K., Lester, M., Jones, T. B., Greenwald, R. A., et al. (1998). SuperDARN studies of the ionospheric convection response to a northward turning of the interplanetary magnetic field. *Annales Geophysicae*, *16*, 549–565. <https://doi.org/10.1007/s00585-998-0549-0>
- Tóth, G., Sokolov, I. V., Gombosi, T. I., Chesney, D. R., Clauer, C. R., De Zeeuw, D. L., et al. (2005). Space weather modeling framework: A new tool for the space science community. *Journal of Geophysical Research*, *110*, A12226. <https://doi.org/10.1029/2005JA011126>
- Tóth, G., van der Holst, B., Igor, S. V., De Zeeuw, D. L., Gombosi, T. I., Fang, F., et al. (2012). Adaptive numerical algorithms in space weather modeling. *Journal of Computational Physics*, *231*, 870–903. <https://doi.org/10.1016/j.jcp.2011.02.006>
- Troshichev, O., Janzhura, A., & Stauning, P. (2006). Unified PCN and PCS indices: Method of calculation, physical sense, and dependence on the IMF azimuthal and northward components. *Journal of Geophysical Research*, *111*, A05208. <https://doi.org/10.1029/2005JA011402>
- Tsurutani, B., Lakhina, G., Verkhoglyadova, O., Gonzalez, W., Echer, E., & Guarnieri, F. (2011). A review of interplanetary discontinuities and their geomagnetic effects. *Journal of Atmospheric and Solar-Terrestrial Physics*, *73*(1), 5–19. <https://doi.org/10.1016/j.jastp.2010.04.001>
- Völk, H. J., & Auer, R.-D. (1974). Motions of the bow shock induced by interplanetary disturbances. *Journal of Geophysical Research*, *79*(1), 40–48. <https://doi.org/10.1029/JA079i001p00040>
- Wang, Y. L., Raeder, J., & Russell, C. T. (2004). Plasma depletion layer: Magnetosheath flow structure and forces. *Annales Geophysicae*, *22*, 1001–1017. <https://doi.org/10.5194/angeo-22-1001-2004>
- Wu, B.-H., Mandt, M. E., Lee, L. C., & Chao, J. K. (1993). Magnetospheric response to solar wind dynamic pressure variations: Interaction of interplanetary tangential discontinuities with the bow shock. *Journal of Geophysical Research*, *98*, 21,297–21,311. <https://doi.org/10.1029/93JA01013>
- Wu, C. C. (1992). MHD flow past an obstacle: Large scale flow in the magnetosheath. *Geophysical Research Letters*, *19*, 87–90. <https://doi.org/10.1029/91GL03007>